

Harbour Oscillation with Bottom Friction

Ikha Magdalena, *Member, IAENG*, Hany Qoshirotur Rif'atin, and Alvedian Mauditra Aulia Matin

Abstract—Theoretically, wave resonance occurs in a harbour when the period of the wave coincides with the harbour's natural resonant period. However, when bottom friction is considered, the resonant period could be affected. Therefore, a model is formulated to simulate the propagation of waves in harbours with bottom friction and used to investigate resonance phenomena in this special case. The governing equations used are the shallow water equations, which are modified to include the friction generated by the interaction between the waves and the harbour's topography. Analytical and numerical approaches are implemented to derive resonant period from the developed model for three geometric harbour types. To validate the numerical model, comparisons against the analytical solutions are provided. Results from both methods turn out to be in very good agreement. The effects of the friction on resonance are analyzed. It is found that bottom friction works well to prevent resonance in rectangular harbours but functions poorly in harbours with triangular profiles.

Index Terms—harbour oscillation, Resonance phenomenon, Bottom friction, Resonant period, Shallow water equations

I. INTRODUCTION

WHEN long waves enter a semi-closed basin connected to the open sea, long-period oscillations called harbour oscillations occur. This phenomenon often occurs in bays, inlets, and fjords, and they may pose dangers to moored ships. Even slight vertical displacements can be followed by significant horizontal harbour currents, whose periods may coincide with the natural resonant period of the ships' swaying motion. Harbour procedures are also disturbed. At worst, such occurrences cause property damage and/or human casualties. Estimating the frequency and amplitude of harbour oscillations is a necessity in the process of designing effective mitigation methods.

The existing literature on this topic includes field measurements [1], [2], experimental studies [3], [4], analytical explorations [5], [6], and studies combining experimental and analytical approaches [7]. Using a multiple-scale perturbation method, Wu and Liu [6] have demonstrated that initial ocean wave groups were able to induce a small-frequency resonant reaction. For cases of harbours of regular shapes, constant depths and friction-less bottoms, linear solutions are well-known [8]–[11]. However, many harbours are of non-regular geometric shapes and have bottoms made of rough material. By formulating the solution as a superposition wave source, Hwang and Tuck [5] were able to derive analytical

approaches for harbours of unspecified plan shape and fixed depth. Lee [7] addressed the same problem using an integral equation. Lee's method approximated the harbour shape by utilizing a matrix equation to define a piece-wise linear boundary of the system. Then, Gerber [12] modified this approach to incorporate dissipation, but only for harbours with flat bottom.

Existing studies [13] provide practical guidelines for predicting the natural resonant periods of harbours based on experimental measurements. Previous analytical studies for harbours with standard shapes and sustained depth corroborate these results. In earlier studies, we have also investigated seiches and harbour oscillations in basins of various two-dimensional geometric shapes [14]–[19]. However, the bottom friction factor has only been considered for the case of seiches in closed basins [20]. The case of harbour oscillations, which occur in semi-closed basins, have not yet been investigated. This study is critical in order to provide a solution in harbours with the potential to experience resonance. Without building additional time- and resource-intensive structures, resonance may be prevented by spreading gravel or other types of rough material over harbour bottoms. The results of this study can factor into considerations on whether or not rough material would be an effective resonance-prevention measure for planned harbour projects.

In our current research, we focus on semi-closed basins constructed using rough materials, taking into account the friction generated by wave movements over the rough base of these basins. This is done in order to closely approximate real harbours. Modern harbour decks are often supported by piles or cantilevered in the direction of the open sea over gabion blocks, resulting in the creation of basins with rough bottoms. A semi-closed rectangular basin can be used to represent harbours with these structural features. Decks may also be supported by natural beaches or sloping revetments, which are walls of masonry or other material erected specifically to provide structural support. A semi-closed parabolic basin can be used to investigate wave propagation near decks supported by beaches, since they often develop concave profiles as they are worn down by waves [21]. We can use a semi-closed triangular basin to approximate decks supported by sloped revetments, as revetments are often arranged to form inclined planes. The materials that make up these structures—often rocks, sand, and wood—are far from smooth, causing there to be friction between their surfaces and the water. Current studies that include analytical results for resonant behavior in these modern harbours neglect this friction effect.

In this paper, we model the movement of waves in each geometric configuration by using the linear shallow water equations (LSWEs). The SWEs have been used in several previous studies to investigate wave propagation in various scenarios. For instance, Magdalena et al. [22] used linear shallow water equations to model wave shoaling. Moreover,

Manuscript received August 5, 2021; revised February 23, 2022. This work was supported by The Ministry of Education, Culture, Research, and Technology of The Republic of Indonesia and ITB.

Ikha Magdalena is a Lecturer and researcher in the Faculty of Mathematics and Natural Sciences, Bandung Institute of Technology, Indonesia (corresponding author; phone: ; fax: ; e-mail: ikha.magdalena@math.itb.ac.id).

Hany Qoshirotur Rif'atin is a research assistant in the Faculty of Mathematics and Natural Sciences, Bandung Institute of Technology, Indonesia (e-mail: hany.qoshirotur@gmail.com).

Alvedian Mauditra Aulia Matin is a research assistant in the Faculty of Mathematics and Natural Sciences, Bandung Institute of Technology, Indonesia (e-mail: a.mauditra@gmail.com).

other researchers extended this work by considering rigid and porous obstacle on modelling fluid flows [23], [24]. Rif'atin and Magdalena [25] have also applied the two-layer shallow water equations to study internal wave propagation over submerged breakwaters. Andadari and Magdalena [26] have implemented the non-linear shallow water equations to simulate wave run-up. In addition to shallow water equations, there are numerous other models used to simulate traveling waves with different conditions. For example, a non-hydrostatic model was used to evaluate wave run-up phenomena and dissipation caused by porous structures [27], [28]. Two-dimensional non-hydrostatic Euler equations were solved using a two-layer approximation in the vertical direction to model a transient wave generated by bottom motion [29]. In addition, the local fractional Boussinesq-type, Burgers-type, and Korteweg-de Vries-type equations have been used to investigate traveling wave solutions for several cases [30]–[37]. Techniques that deal with the difficulties presented by the higher-order and nonlinear terms of Boussinesq-type and Burgers-type equations [38]–[40] as well as Korteweg-de Vries-type equations [41], [42] can be found in the literature. Several models can be used to evaluate resonant waves over topographies with bottom friction. However, the linear shallow water equations were chosen for this study, as they are sufficient for modeling the resonant period and amplitude of the wave. We do not investigate the wave profile or the wave's non-linear properties. Moreover, linear shallow water equations are significantly easier solve, both analytically and numerically. Their ability to model resonance accurately has also been proven by several previous studies [14], [15], [20]. The shallow water equations are therefore considered appropriate for this study. Analytical approaches are used to determine the resonant period for each case with bottom friction. We also formulate a numerical scheme that can be used in scenarios of arbitrarily shaped geometry. The analytical and numerical solutions will be examined and compared to evaluate the impacts of a friction coefficient on reducing wave resonant period and its maximum amplitude.

This paper is structured in the following way. In Section 2, we present the model we use to describe physical movements of a wave, while the derivations of the analytical natural resonant period in each type of basin with friction are explained in Section 3. We present a computational scheme based on the staggered finite volume method in Section 4. The computational results are shown and compared to those of the analytical solutions in Section 5. A brief conclusion is then provided in Section 6.

II. MATHEMATICAL MODEL

Here, a model of wave flow over rough topography is constructed using the well-known Linear Shallow Water Equations (LSWEs). First, we consider a wave propagating into a harbour as depicted in Figure 1. In this scenario, we assume that the harbour has a rough bottom. The incoming wave travels from the ocean to the harbour, thus entering the domain from the right. Meanwhile, the left-side border of the domain represents a rigid wall. The term $\eta(x, t)$ describes the elevation of the surface wave, $u(x, t)$ denotes the wave velocity in horizontal direction, and $h = \eta + d$ is the thickness of the water body. Here, we presume that the value of η is much smaller than h , so we may rewrite the water thickness

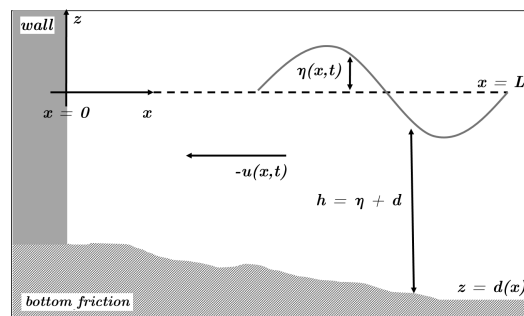


Fig. 1. Wave flow over a rough topography described by the Shallow Water Equations.

as $h \approx d$, where d is the water depth measured at the undisturbed water condition.

We now modify the LSWEs to take into account bottom friction induced by wave-topography interaction. The adjustment is done by incorporating $C_f u$, an element representing bottom friction, into the momentum equation [43]. Consequently, the model can be written as

$$\eta_t + (hu)_x = 0, \quad (1)$$

$$u_t + g\eta_x + C_f u = 0, \quad (2)$$

in which $g (= 9.81 m/s^2)$ denotes acceleration due to gravity and C_f is the friction coefficient.

In this study, Equations (1, 2) are solved analytically and numerically for harbours of three common geometric types:

- Rectangular harbour with depth of $h(x) = h_1$,
- Triangular harbour with depth of $h(x) = h_1 \frac{x}{L}$,
- Semi-parabolic harbour with depth of $h(x) = h_1 (1 - \frac{x^2}{L^2})$,

in which h_1 is the maximum depth of each topography.

III. ANALYTICAL SOLUTIONS

This section explains the analytical solution for equations (1) and (2), obtained using separation of variables. The solution allows us determine the wave's natural resonant frequency as it travels across harbours of various topographies. Assuming that the wave is monochromatic, we may define two functions $F(x)$ and $G(x)$

$$\eta(x, t) = F(x)e^{-i\omega t}, \quad (3)$$

$$u(x, t) = G(x)e^{-i\omega t}. \quad (4)$$

The wave resonant frequency ω can then be determined by analytically solving differential equations in terms of $F(x)$. The following cases may now be observed.

- Rectangular harbour with depth $h(x) = h_1$

In this case, $h(x) = h_1$. Equations (3) and (4) are then substituted into (1) and (2). Thus we obtain the following equations describing the motion of the wave in a rectangular harbour.

$$-i\omega F(x) + h_1 G_x(x) = 0, \quad (5)$$

$$-i\omega G(x) + gF_x(x) + C_f G(x) = 0. \quad (6)$$

Algebraic manipulation then yields the following expressions.

$$G(x) = \frac{g}{i\omega - C_f} F_x(x), \quad (7)$$

$$G_x(x) = \frac{g}{i\omega - C_f} F_{xx}(x). \quad (8)$$

With substitution, the equation (4) may be written as

$$-i\omega F(x) + \frac{h_1 g}{i\omega - C_f} F_{xx}(x) = 0, \quad (9)$$

From this we obtain $F(x)$.

$$F(x) = c_1 e^{ikx} + c_2 e^{-ikx}. \quad (10)$$

The wave number k follows the dispersion relation $k^2 = \frac{\omega^2 + i\omega C_f}{gh_1}$. We can then derive the above expression with respect to x to obtain

$$F_x(x) = ik(c_1 e^{ikx} - c_2 e^{-ikx}). \quad (11)$$

The boundary condition $F_x(0) = 0$ implies $c_1 = c_2$. The boundary condition $F(L) = 0$ allows us to find kL .

$$c_1(e^{ikL} + e^{-ikL}) = 0, \\ 2\cos(kL) = 0.$$

Thus $kL = \frac{(2n-1)\pi}{2}$ with $n \in \mathbb{N}$. We choose $n = 1$ in order to arrive at a fundamental solution. This gives us

$$\left(\sqrt{\frac{\omega^2 + i\omega C_f}{gh_1}} \right) L = \frac{\pi}{2},$$

and thus

$$\omega^2 + iC_f\omega = \frac{\pi^2 gh_1}{4L^2}. \quad (12)$$

Let $\omega_0^2 = \frac{\pi^2 gh_1}{4L^2}$ be the squared wave frequency when there is no friction force involved.

$$\omega = A_0 \pm \sqrt{A_0^2 + \omega_0^2}, \quad (13)$$

with $A_0 = |-\frac{iC_f}{2}|$. Since A_0 and ω_0 are equal to or larger than zero and $\omega \geq 0$,

$$\omega = A_0 + \sqrt{A_0^2 + \omega_0^2}. \quad (14)$$

(b) Triangular harbour with depth $h(x) = h_1 \frac{x}{L}$.

As in the rectangular case, we can obtain equations to describe the wave's motion by substituting the defined expression for $h(x)$ and equations (3) and (4) to (1) and (2).

$$-i\omega F + hG_x + h_x G = 0, \quad (15)$$

$$-i\omega G + gF_x + C_f G = 0. \quad (16)$$

And thus

$$G(x) = \frac{g}{i\omega - C_f} F_x, \quad (17)$$

$$G_x(x) = \frac{g}{i\omega - C_f} F_{xx}. \quad (18)$$

We then substitute these equations into (15) to obtain

$$-i\omega F + \frac{hg}{i\omega - C_f} F_{xx} + \frac{g}{i\omega - C_f} F_x = 0. \quad (19)$$

The solution to this second-order differential equation is

$$F(x) = c_3 J_0(\alpha(x)) + c_4 Y_0(\alpha(x)). \quad (20)$$

$J_0(\alpha(x))$ is the zeroth-order first kind Bessel function, $Y_0(\alpha(x))$ is the zeroth-order second kind Bessel function, and $\alpha(x) = 2\sqrt{\frac{x i\omega L(-i\omega + C_f)}{h_1 g}}$. The first derivative of $F(x)$ is

$$F_x(x) = c_3 J_1(\alpha(x)) \frac{\alpha(x)}{2x} + c_4 Y_0(\alpha(x)). \quad (21)$$

The boundary conditions are defined as $F_x(0) = 0$ and $F(L) = 0$, and it is known that $\lim_{x \rightarrow \infty} Y_1(x) = \alpha(0)$, therefore $c_4 = 0$. This allows the first boundary condition to be satisfied. To find c_3 , we use the boundary condition $F(L) = 0$. Observe that

$$c_3 J_1(\alpha(L)) = 0,$$

$$J_1(\alpha(L)) = 0,$$

$$\alpha(L) = 2.4048,$$

$$2L \sqrt{\frac{i\omega(-i\omega + c_f)}{h_1 g}},$$

which gives us

$$\omega^2 + iC_f\omega = \left(\frac{2.4048\sqrt{h_1 g}}{2L} \right)^2. \quad (22)$$

Let $\omega_0^2 = \left(\frac{2.4048\sqrt{h_1 g}}{2L} \right)^2$ be the wave resonant frequency over a friction-less surface. Applying the quadratic formula and the information that $\omega \geq 0$, we now have

$$\omega = A_0 + \sqrt{A_0^2 + \omega_0^2}, \quad (23)$$

with $A_0 = |-\frac{iC_f}{2}|$.

(c) Semi-parabolic harbour with depth $h(x) = h_1(1 - \frac{x^2}{L^2})$. When we substitute $h(x)$ as well as the equations (3) and (4) to (1) and (2), we obtain equations (15) and (16). This time, however, $h(x) = h_1(1 - \frac{x^2}{L^2})$ and $h_x(x) = \frac{-2x}{L^2} h_1$. We can then find the solution to the second-order differential equation (19),

$$F(x) = c_5 P_\gamma\left(\frac{x}{L}\right) + c_6 Q_\gamma\left(\frac{x}{L}\right), \quad (24)$$

with $\gamma = -\frac{1}{2} \left(1 - \sqrt{\frac{4L^2(\omega^2 + i\omega C_f)}{gh_1} + 1} \right)$. Here, the functions P and Q are the Legendre function of the first and second kind, respectively.

From the first derivative of $F(x)$ and the boundary condition $F_x(-L) = 0$, we can see that

$$c_5 \left(P_{\gamma+1}(-1) + P_\gamma(-1) \right) + c_6 \left(Q_{\gamma+1}(-1) + Q_\gamma(-1) \right) = 0.$$

Since $Q_\gamma(-1) = \infty$ for $\gamma = 0, 1, 2, \dots$, the value of c_6 must be zero. In order for a non-trivial solution to be found, the following must apply:

$$P_{\gamma+1}(-1) = -P_\gamma(-1). \quad (25)$$

We know that $P_\gamma(-1) = (-1)^\gamma$ for every $\gamma = 0, 1, 2, \dots$, and thus equation (25) will always be fulfilled. We choose the smallest non-zero value of γ , 1, to obtain the fundamental solution.

This allows us to obtain

$$-\frac{1}{2} \left(1 - \sqrt{\frac{4L^2(\omega^2 + i\omega C_f)}{gh_1} + 1} \right) = 1,$$

and thus

$$\omega^2 + iC_f\omega = \frac{2gh_1}{L^2}. \quad (26)$$

Let $\omega_0^2 = \frac{2gh_1}{L^2}$ be the squared resonant wave frequency when friction is ignored. Solving Equation (26) with the knowledge that $\omega > 0$, we obtain

$$\omega = A_0 + \sqrt{A_0^2 + \omega_0^2}. \quad (27)$$

IV. NUMERICAL METHOD

We apply a finite volume method on a staggered grid to numerically solve the modified LSWEs model. Let $[0, L]$ be our observation domain. The numerical domain is then divided into $0 = x_{1/2}, x_1, x_{3/2}, x_2, \dots, x_{N-1/2}, x_N, x_{N+1/2} = L$ as illustrated in Figure 2.

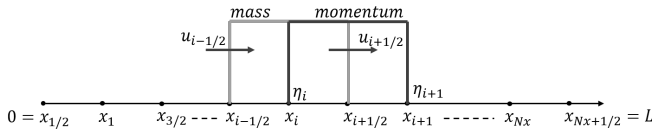


Fig. 2. Description of the finite volume method on a staggered grid.

The mass conservation equation (1) is approximated at cells centered on points labeled x_{i+1} . Meanwhile, momentum equation (2) is computed at cells centered on points labeled $x_{i+1/2}$, with $i = 0, 1, 2, 3, \dots, Nx-1, Nx$. Values of η and h are computed only at x_{i+1} (full-grid points) using equation (1) which is the mass conservation equation. Values of u are calculated only at $x_{i+1/2}$ (half-grid points) using momentum equation (2). The resulting numerical scheme is written below.

$$\frac{\eta_i^{n+1} - \eta_i^n}{\Delta t} + \frac{(hu)_{i+1/2}^n - (hu)_{i-1/2}^n}{\Delta x} = 0 \quad (28)$$

$$\frac{u_{i+1/2}^{n+1} - u_{i+1/2}^n}{\Delta t} + g \frac{\eta_{i+1}^{n+1} - \eta_i^{n+1}}{\Delta x} + C_f u_{i+1/2}^{n+1} = 0 \quad (29)$$

Notice that the scheme requires the value of hu at half-grid points $x_{i+1/2}$. However, h is only defined at full-grid points. Thus a first-order upwind method is proposed to approximate value of h is at every half-grid point. The mathematical expression for the method is as follows.

$$h_{i+1/2}^n = \begin{cases} h_i^n, & \text{for } u_{i+1/2}^n \geq 0, \\ h_{i+1}^n, & \text{for } u_{i+1/2}^n < 0 \end{cases} \quad (30)$$

Now, we have a numerical scheme consisting of equations (28) and (29), which is complemented by equation (30). Together, these expressions allow us to obtain a numerical solution for our model. Note that the friction term $C_f u$ is approximated implicitly by $C_f u_{i+1/2}^{n+1}$. This is done to avoid a more restrictive stability condition. The stability condition for this scheme is the same as that for the LSWEs without bottom friction. This condition, obtained using Von Neumann stability analysis, is expressed as $\sqrt{gh_1} \frac{\Delta t}{\Delta x} \leq 1$. Moreover, the numerical scheme detailed in equations (28) and (29) has no damping error [44].

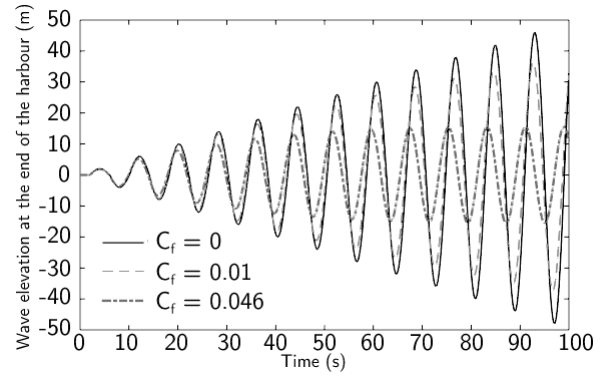


Fig. 3. Resonance phenomenon in a rectangular harbour with different values of C_f .

Using (28), (29), and (30), we simulate wave flow in a harbour with rough topography. All the simulation results are then validated with analytical solutions obtained in Section III.

V. RESULTS AND DISCUSSION

Here, the computational scheme developed in Section III is implemented to replicate wave resonance occurrence in harbours with rectangular, triangular, and semi-parabolic profiles. Bottom friction is assumed to be present in every case. Later in this section, we will analyze the numerical results to study how resonance occurs in various topography types, particularly when bottom friction is applied.

The simulations in this section are conducted with an observational domain of $[0, 20]$ m and are observed for $T = 100$ s. The observational domain is partitioned into sections with the length $\Delta x = 0.1$ m. The time step for each iteration is $\Delta t = \Delta x / \sqrt{gH_1}$ s. The bottom topography for each type follows the expression for $h(x)$ stated in Section 3 with a maximum depth of $H_1 = 10$ m. To match the conditions of real harbours, we configure the right boundary as a hard wall or $u(L, t) = 0$. At $x = 0$, we have an open boundary. A harmonic wave enters the port from this side with an initial amplitude of $A_i = 1$ m and an angular frequency of ω , in line with the analytical solutions in Section 3. Using these parameters, the simulation results for each kind of harbour with various values of C_f are shown in Figure (3-5). In each figure, the wave profiles are captured at the end of the domain ($x = 20$) at every time step.

Before addressing the aspects visually illustrated in Figures (3-5), we must first evaluate the numerically-obtained natural resonant periods of the different harbour types by comparing them to analytically-derived resonant periods. The comparisons between analytically-derived and numerically-obtained resonant periods are outlined in Table (I).

Table (I) presents the analytical values of T_1 , calculated using the analytical solutions of ω , with $T_1 = 2\pi/\omega$ s. For each harbour shape, we determine the numerical and analytical T_1 with three values of C_f and then compare those two values to analyze the accuracy of our numerical simulations relative to our analytical solutions. For $C_f = 0$, which is the case of a harbour without bottom friction, the comparison for each harbour was presented in a previous study [15]. Only a very small error exists between the analytical and numerical results.

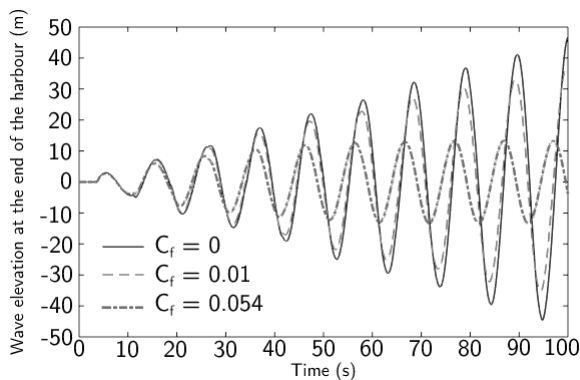


Fig. 4. Resonance phenomenon in a triangular harbour with different values of C_f .

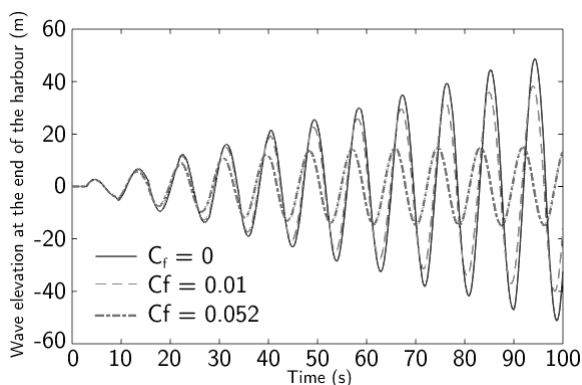


Fig. 5. Resonance phenomenon in a semi-parabolic harbour simulated using the LSWEs computational scheme with different values of C_f .

Now, in the case of bottom friction, there are two cases presented here: resonance and non-resonance scenarios. When we run the simulation with $C_f = 0.01$, as described in Figures (3-5), resonance is still present. On the other hand, resonance is not seen in the simulation results where $C_f = f_0$ for each harbour. We set $f_0 = 0.046$ for the rectangular harbour, $f_0 = 0.054$ for the triangular harbour, and $f_0 = 0.052$ for the semi-parabolic harbour. The difference in this non-resonance situation will be explained further in the end part of this section. However, for the case of resonance, Table (I) shows that the analytical and computational resonant periods are in very good quantitative agreement. We are able to draw this conclusion by first calculating the relative error using the formula $error = \left| \frac{T_{1numeric} - T_{1analytic}}{T_{1analytic}} \right| \times 100\%$. The reported errors are the average relative errors between analytical and numerical T_1 for each bottom topography and all three values of C_f . These values are less than or equivalent to 0.5%. These relatively small errors indicate that our numerical scheme models resonance phenomenon very well.

We now examine how much bottom friction affects resonance in each harbour type. This bottom friction effect can be investigated by looking at two aspects: the minimum resonance-preventing value of C_f and the changes in growth rate when C_f is adjusted. For resonance-preventing values of C_f , we may analyze this feature from Figures (3-5). These figures show that resonance occurs even when the friction coefficient's magnitude is increased, for example when we define $C_f = 0.01$. At some point, however, friction can

TABLE I
RESULTS COMPARISON BETWEEN THE ANALYTICALLY-DERIVED AND NUMERICALLY-OBTAINED RESONANT PERIODS IN EACH HARBOUR.

| Harbour's type | C_f values | Analytical T_1 (s) | Numerical T_1 (s) | Error (%) |
|----------------|--------------|----------------------|---------------------|-----------|
| Rectangular | 0 | 8.077 | 8.087 | 0.124 |
| | 0.01 | 8.025 | 8.059 | 0.424 |
| | 0.046 | 7.842 | 7.917 | 0.956 |
| Triangular | 0 | 10.552 | 10.518 | 0.322 |
| | 0.01 | 10.464 | 10.467 | 0.029 |
| | 0.054 | 10.084 | 10.176 | 0.912 |
| Semi-parabolic | 0 | 8.971 | 8.971 | 0 |
| | 0.01 | 8.907 | 8.933 | 0.292 |
| | 0.052 | 8.644 | 8.730 | 0.995 |

TABLE II
CHANGES OF THE GROWTH RATES OF WAVE AMPLITUDE DUE TO RESONANCE FOR EVERY HARBOUR WHEN $C_f = 0$ AND $C_f = 0.01$.

| Harbour's type | Growth rate ($\%s^{-1}$) | | Growth rate changes ($\%s^{-1}$) |
|----------------|----------------------------|--------------|------------------------------------|
| | $C_f = 0$ | $C_f = 0.01$ | |
| Rectangular | 24.695 | 19.463 | 5.232 |
| Triangular | 15.356 | 12.306 | 3.050 |
| Semi-parabolic | 19.166 | 15.071 | 4.095 |

stop resonance from occurring, and this resonance-preventing value of C_f is specific for each harbour shape. A non-resonance state is indicated by the appearance of a declining pattern after the wave reaches its peak amplitude. With regards to this criterion, the port types may be listed in ascending order of resonance-avoiding C_f : rectangular, semi-parabolic, and triangular. The resonance-avoiding C_f values of each type are $C_f = 0.046, 0.052,$ and $0.054,$ respectively. This result implies that compared to the amount needed in triangular and semi-parabolic harbours, the amount of friction required to avoid resonance is fairly low in rectangular harbours. This suggests that bottom friction works best as a resonance-preventing measure in rectangular harbours and it does not work very well in triangular harbours. This statement is supported by the changes in wave amplitude growth rates when C_f is varied.

Table (II) displays wave amplitude growth rates in all harbour types. These growth rates are calculated using two different values of friction coefficient. The value $C_f = 0$ represents the absence of friction force and $C_f = 0.01$ is used to investigate the case where bottom friction is present. The amplitude growth rates are calculated using the linear growth rate formula $growth\ rate = \left| \frac{Crest_F - Crest_I}{Crest_I} \right| \times \left| \frac{1}{t_F - t_I} \right| \times 100\%$. $Crest_F$ denotes the value of the last crest point of each wave in Figures (3-5), while $Crest_I$ is the first crest point of each wave. The terms t_F and t_I refer to values of t that coincide with the appearances of $Crest_F$ and $Crest_I$, respectively. Table (II) also informs us how differently the growth rates drop in each harbour type when we set the same value of $C_f = 0.01$. When C_f is constant, the growth rate in the rectangular harbour decreases the most, followed by that of the semi-parabolic type. The growth rate in the triangular harbour undergoes the smallest decline. It can be concluded that bottom friction has more impact on resonance in rectangular harbours compared to the other two types. This is consistent with our previous result, which indicates that a smaller C_f value is needed to prevent resonance. On the other hand, a greater C_f value is required to prevent resonance in triangular harbours as

bottom friction has a smaller impact on resonance. These conclusions support the previous claims regarding bottom friction effectiveness for the different harbour types.

VI. CONCLUSION

By modifying the linear shallow water equations and adding a term representing bottom friction to the momentum equation, resonance in a harbour with a rough bottom can be modeled. The model is constructed for three different harbour types: rectangular, triangular, and semi-parabolic. The modified model is then solved analytically to determine the general formula for the natural resonant period of waves propagating in harbours with bottom friction expressed in terms of the natural resonant period of waves propagating in harbours with no bottom friction. The natural resonant periods for harbours with friction decrease as the friction coefficient grows. A finite volume method on a staggered grid is applied to formulate a numerical model of wave resonance in a rough harbour. The computationally-obtained resonant periods are then compared against the corresponding analytical solutions to validate the numerical scheme. The comparison shows a very good agreement between the two solutions, with relatively small errors within the range of 0 to 0.5 percent. The results show that a relatively small value of C_f is sufficient to prevent resonance in rectangular harbours. Thus, bottom friction works best as a resonance-prevention measure in rectangular harbours. In contrast, the triangular harbour requires a larger value of C_f to prevent resonance from occurring, leading us to conclude that bottom friction performs poorly as a method of resonance prevention in this type of harbour.

REFERENCES

- [1] I. Melito, G. Cuomo, G. Bellotti, and L. Franco, "Field measurements of harbor resonance at marina di carrara," *Proceedings of the Twenty-third International Conference of Coastal Engineering*, pp. 1280–1292, 2006.
- [2] I. Vilibic and H. Mihanovic, "A study of resonant oscillations in the split harbour (adriatic sea)," *Estuar. Coast. Shelf Sci.*, vol. 56 (3-4), pp. 861–867, 203.
- [3] P. D. Girolamo, "An experiment on harbor resonance induced by incident regular and irregular short waves," *Coast. Eng.*, vol. 27, pp. 47–66, 1996.
- [4] F. M. Martinez and V. S. Naverac, "An experimental study of harbor resonance phenomena," *Proceedings of the Twenty-first International Conference on Coastal Engineering*, pp. 1280–1292, 1988.
- [5] L. S. Hwang and E. O. Tuck, "On the oscillations of harbours of arbitrary shape," *J. Fluid Mech.*, vol. 42, pp. 447–464, 1970.
- [6] J.-K. Wu and P.-F. Liu, "Harbour excitations by incident wave groups," *J. Fluid Mech.*, vol. 217, pp. 595–613, 1990.
- [7] J.-J. Lee, "Wave-induced oscillations in harbours of arbitrary geometry," *J. Fluid Mech.*, vol. 45, pp. 375–394, 1971.
- [8] A. E. Gill, *Atmosphere-Ocean Dynamics*. London: Academic Press, 1982, p. 30.
- [9] D. E. Reeve, A. J. Chadwick, and C. A. Fleming, *Coastal Engineering: Processes, Theory and Practice, 3rd ed.* London: CRC Press, 2018.
- [10] C. C. Mei, *The Applied Dynamics of Ocean Surface Waves*. Singapore: World Scientific, 1989, p. 1.
- [11] B. Wilson, *Chapter: Seiches in Advances in Hydrosience*. Cambridge, America: Academic Press, 1972, vol. 8, pp. 1–93.
- [12] M. Gerber, "Modelling dissipation in harbour resonance," *Coast. Eng.*, vol. 10, pp. 211–252, 1986.
- [13] A. Rabinovich, *Chapter 9: Seiches and Harbor Oscillations in Handbook of Coastal and Ocean Engineering (edited by Y. C. Kim)*. Singapore: World Scientific Publ., 2009, pp. 193–236.
- [14] H. Q. Rif'atin and I. Magdalena, "Seiches in a closed basin of various geometric shape," *Journal of Physics: Conference Series*, vol. 1245, p. 012061, aug 2019.
- [15] I. Magdalena, H. Q. Rif'atin, and D. E. Reeve, "Seiches and harbour oscillations in a porous semi-closed basin," *Appl. Math. Comput.*, vol. 369, p. 124835, 2020.
- [16] I. Magdalena, N. Karima, and H. Rif'atin, "A mathematical model for investigating the resonance phenomenon in lakes," *Wave Motion*, vol. 100, p. 102669, 01 2021.
- [17] I. Magdalena, N. Karima, and H. Rif'atin, "Analytical and numerical studies for seiches in a closed basin with various geometric shapes of longitudinal section," *Theoretical and Applied Mechanics Letters*, p. 100246, 2021.
- [18] I. Magdalena, N. Karima, and H. Q. Rif'atin, "Resonant periods of seiches in semi-closed basins with complex bottom topography," *Fluids*, vol. 6, no. 5, 2021.
- [19] I. Magdalena and H. Rif'atin, "Analytical and numerical studies for harbor oscillation in a semi-closed basin of various geometric shapes with porous media," *Mathematics and Computers in Simulation*, vol. 170, pp. 351–365, 2020. [Online]. Available: <https://www.sciencedirect.com/science/article/pii/S0378475419303337>
- [20] I. Magdalena, H. Rif'atin, and A. M. A. Matin, "Analytical and numerical studies for seiches in a closed basin with bottom friction," *Theoretical and Applied Mechanics Letters*, vol. 10, no. 6, pp. 429–437, 2020.
- [21] R. G. Dean, "Equilibrium beach profiles: characteristics and applications," *J. Coast. Res.*, vol. 7, pp. 53–84, 1991.
- [22] I. Magdalena, I. Iryanto, and D. Reeve, "Free-surface long wave propagation over linear and parabolic transition shelves," *Water Science and Engineering*, vol. 11, 01 2019.
- [23] I. Magdalena and M. Roque, "Analytical and numerical solution for wave reflection from a porous wave absorber," *Journal of Physics: Conference Series*, vol. 974, p. 012042, 03 2018.
- [24] I. Magdalena, M. Atras, L. Sembiring, A. Nugroho, R. Labay, and M. Roque, "Wave transmission by rectangular submerged breakwaters," *Computation*, vol. 8, p. 56, 06 2020.
- [25] H. Rif'atin and I. Magdalena, "Internal wave propagation in a two-fluid rigid lid system over submerged bars," *Journal of Physics: Conference Series*, vol. 1321, p. 032118, 10 2019.
- [26] G. Andadari and I. Magdalena, "Analytical and numerical studies of resonant wave run-up on a plane structure," *Journal of Physics: Conference Series*, vol. 1321, p. 022079, 10 2019.
- [27] I. Magdalena and N. Erwina, "An efficient two-layer non-hydrostatic model for investigating wave run-up phenomena," *Computation*, vol. 8, no. 1, 2020.
- [28] I. Magdalena, "Non-hydrostatic model for solitary waves passing through a porous structure," *Journal of Disaster Research*, vol. 11, pp. 957–963, 10 2016.
- [29] S. R. Pudjaprasetya, I. Magdalena, and S. S. Tjandra, "A nonhydrostatic two-layer staggered scheme for transient waves due to anti-symmetric seabed thrust," *Journal of Earthquake and Tsunami*, vol. 11, no. 01, p. 1740002, 2017.
- [30] X.-J. Yang, J. A. T. Machado, and D. Baleanu, "Exact traveling-wave solution for local fractional Boussinesq equation in fractal domain," *Fractals*, vol. 25, p. 1740006, 2017.
- [31] X.-J. Yang, F. Gao, and H. M. Srivastava, "Exact travelling wave solutions for the local fractional two-dimensional Burgers-type equations," *Computers and Mathematics with Applications*, vol. 73, pp. 203–210, 2017.
- [32] X.-J. Yang, J. A. T. Machado, D. Baleanu, and C. Cattani, "On exact traveling-wave solutions for local fractional Korteweg-de Vries equation," *Chaos: An Interdisciplinary Journal of Nonlinear Science*, vol. 26, p. 084312, 2016.
- [33] Y. Xiao-Jun, J. Hristov, H. Srivastava, and B. Ahmad, "Modelling fractal waves on shallow water surfaces via local fractional Korteweg-de Vries equation," *Abstract and Applied Analysis*, vol. 2014, 05 2014.
- [34] S. Ye, S. MOHYUD-DIN, and F. Belgacem, "The laplace series solution for local fractional Korteweg-de Vries equation," *Thermal Science*, vol. 20, pp. 867–870, 08 2016.
- [35] Y. Wang, Y. F. Zhang, and Z. J. Liu, "An explanation of local fractional variational iteration method and its application to local fractional modified Korteweg-de Vries equation," vol. 22, pp. 23–27, 2018.
- [36] Y. J. Yang and S. Q. Wang, "A local fractional homotopy perturbation method for solving the local fractional Korteweg-de Vries equations with non-homogeneous term," vol. 23, pp. 1495–1501, 2019.
- [37] F. Gao, X.-J. Yang, and Y. Ju, "Exact traveling-wave solutions for one-dimensional modified Korteweg-de Vries equation defined on cantor sets," *Fractals*, vol. 27, no. 01, p. 1940010, 2019.
- [38] S. Chonladed and K. Wuttanachamsri, "A numerical solution of Burger's equation based on Milne method," *IAENG International Journal of Applied Mathematics*, vol. 51, no. 2, pp. 411–415, 2021.
- [39] J. Zuo, "Bäcklund transformations and exact explicit solutions for a high-order classical Boussinesq-Burgers equation," *IAENG Interna-*

- tional Journal of Applied Mathematics*, vol. 49, no. 4, pp. 495–499, 2019.
- [40] J. Zuo, “Cte method and exact solutions for a high-order Boussinesq-Burgers equation,” *IAENG International Journal of Applied Mathematics*, vol. 50, no. 2, pp. 440–444, 2020.
- [41] J.-L. Yan and L.-H. Zheng, “New energy-preserving finite volume element scheme for the Korteweg-de Vries equation,” *IAENG International Journal of Applied Mathematics*, vol. 47, no. 2, pp. 223–232, 2017.
- [42] J.-L. Yan and L.-H. Zheng, “A class of momentum-preserving Fourier pseudo-spectral schemes for the Korteweg-de Vries equation,” *IAENG International Journal of Applied Mathematics*, vol. 49, no. 4, pp. 548–560, 2019.
- [43] R. G. Dean and R. A. Dalrymple, *Water Wave Mechanics for Engineer and Scientists in Advanced Series on Ocean Engineering - Volume 2*, P. L.-F. Liu, Ed. Singapore: World Scientific, 1991.
- [44] S. Pudjaprasetya and I. Magdalena, “Momentum conservative schemes for shallow water flows,” *East Asian J. on Appl. Math.*, vol. 4, pp. 152–165, 2014.

Ikha Magdalena is a Lecturer at Institut Teknologi Bandung’s Department of Mathematics. She conducts research on fluid dynamics, wave models, numerical modeling, and coastal protection. Her research has been published in Q1 Journal, and other reputable mathematics and engineering Journals. Since the beginning of her career as a researcher, she has been awarded numerous grants from the Indonesian Ministry of Research, Technology, and Higher Education as well as from Institut Teknologi Bandung. She received an Award in Industrial and Academia Partnership from Royal Academy of Engineering, the Individual Researcher Links Award from the British Council and a grant from the Newton Fund. She is also the creator of Wave Interaction with Vegetation, a copyrighted fluid modeling software, and she actively manages ITB’s Research Center for Coastal and Ocean. She believes in the power of collaboration in research, and works on research problems with colleagues from Indonesia, the UK, the Philippines, China, India and the Netherlands. Aside from joint projects, she maintains active participation in mathematical societies. Since 2014, she has been heavily involved in the management of the Indonesian Mathematical Society (IndoMS) and now serves as its Coordinator of International Collaborations. She is a member of the Silkroad Mathematics Center’s Steering Committee and the Executive Committee of the Society for Industrial and Applied Mathematics (SIAM). She is the faculty advisor of SIAM Student Chapter ITB.